

> REPLACE THIS LINE WITH YOUR PAPER IDENTIFICATION NUMBER (DOUBLE-CLICK HERE TO EDIT) <

The following publication M. Ghafouri, U. Karaagac, H. Karimi, S. Jensen, J. Mahseredjian and S. O. Faried, "An LQR Controller for Damping of Subsynchronous Interaction in DFIG-Based Wind Farms," in IEEE Transactions on Power Systems, vol. 32, no. 6, pp. 4934-4942, Nov. 2017 is available at <https://doi.org/10.1109/TPWRS.2017.2669260>.

An LQR Controller for Damping of Subsynchronous Interaction in DFIG-Based Wind Farms

M. Ghafouri, Student Member, IEEE, U. Karaagac, Member, IEEE, H. Karimi, Senior Member, IEEE, S. Jensen, Member, IEEE, J. Mahseredjian, Fellow, IEEE, S.O. Faried, Senior Member, IEEE

Abstract— This paper presents a linear-quadratic regulator (LQR) for damping of subsynchronous interaction (SSI) in doubly-fed induction generator (DFIG)-based wind farms. The proposed LQR controller employs a full-state observer to estimate all state variables. The output of the LQR is added to control signals of inner current control loops of DFIG converters as supplementary control signals. The supplementary control signals are dynamically limited to avoid saturating the converters and to provide the DFIG with the desired transient response against power system faults. The proposed SSI damping controller is designed for a realistic series compensated wind farm, and its performance is verified using electromagnetic transient (EMT) simulations. The EMT simulations are performed using a detailed DFIG model which includes all nonlinearities and all required transient functions to meet the grid code requirements corresponding to fault-ride-through (FRT). The results show that the proposed SSI controller is able to significantly mitigate the oscillations due to the SSI phenomenon, and to provide excellent transient response against systems faults.

Index Terms— Doubly-fed induction generator (DFIG), observer design, optimal control, series capacitor compensation, subsynchronous interaction (SSI), wind farm.

I. INTRODUCTION

Recent studies recognize the susceptibility of doubly-fed induction generator (DFIG)-based wind farms connected to series capacitor compensated transmission lines to subsynchronous interaction (SSI) [1]-[2]. This was confirmed in October 2009 with the occurrence of the first SSI incident in the Zorillo Gulf wind farm in Texas [3]-[4]. Since that incident, there has been a growing interest in developing effective SSI mitigation methods [5]-[13][12].

The SSI mitigation methods based on supplementary control signals in DFIG control [7]-[12] are quite promising due to their low investment costs. However, further research is required to conclude on the effectiveness and/or feasibility of the existing methods, e.g. [8]-[12], due to the following reasons:

- Time domain simulations in [8]-[12] are performed using simple linear DFIG models for verifying the proposed SSI damping controller performance. Those simple DFIG

models do not include the nonlinearities and the transient functions to achieve the grid code requirements corresponding to fault-ride-through (FRT). Hence, the potential adverse effects of SSI damping controller on FRT operation performance (or vice versa) is totally disregarded in [8]-[12].

- According to customary grid code requirements, the wind farm should have a WFC to control the reactive power at point of interconnection (POI). The wind farm reactive power control is based on the secondary voltage control concept. At primary level, the wind turbine controller monitors and controls its own terminal voltage with a proportional voltage regulator. At secondary level, the WFC monitors the reactive power at POI and control it by modifying the wind turbine controller reference voltage values via a proportional-integral (PI) reactive power regulator. The wind farm reactive power control schemes in [8][13] are not realistic as they disregard the central wind farm controller (WFC).

The proposed SSI damping method of this paper overcomes the aforementioned drawbacks of the existing methods. Unlike [8]-[11][13], the detailed electromagnetic transient (EMT) models of DFIG in [7],[14] include the essential transient functions to fulfill the grid code requirements regarding FRT [15]. In the investigations conducted in [7], the SSI damping controller output is blocked when the FRT function of DFIG is activated to achieve the desired transient response. However, blocking SSI damping controller during fault may significantly deteriorate the performance of the damping method especially when the faulted system has an undamped SSI mode. Therefore, the blocking (or restricting) of SSI damping controller output signals should carefully be examined considering the extreme fault scenarios.

The linear-quadratic regulator (LQR) method has been widely used in power system control due to its simplicity and robustness [16],[17]. This paper proposes a linear-quadratic regulator (LQR) to damp the oscillations due to the SSI phenomena, and to ensure safe operation of DFIG-based wind

M. Ghafouri, H. Karimi and J. Mahseredjian are with Polytechnique Montreal, Montreal (Quebec), Canada; U. Karaagac is with The Hong Kong Polytechnic University, Hong Kong; S. Jensen is with Servion SE, Hamburg, Germany; S.O. Faried is with University of Saskatchewan, Saskatoon (Saskatchewan), Canada.

farms connected to a series capacitor compensated transmission network. The SSI damping controller includes a full state observer to estimate the state variables, and an LQR-based state feedback controller. The model used for the control design is a reduced order system with 22 state variables, and is obtained by neglecting the dynamics with marginal effect on the SSI mode.

The proposed controller receives the currents of the rotor side converter (RSC) and the grid side converter (GSC) of the DFIG, as its inputs. The output signals of the SSI damping controller are supplemented to the inner current control loops of the DFIG converters. These supplementary signals are dynamically limited to keep the RSC and GSC in the linear regions, and to provide the desired transient response for the DFIG against the faults. In this paper, the linear matrix inequality (LMI) technique is used to design the observer gain.

The performance of the proposed SSI damping controller is validated by means of EMT simulations. The DFIG-based wind farm used in the EMT simulations is a realistic detailed model which includes the nonlinearities (in both electrical and control systems) and the FRT function. Unlike the existing SSI mitigation methods, both the linearized and the realistic EMT models used in this paper include the central wind farm controller (WFC), i.e. the centralized reactive power control scheme is considered. The EMT simulation results show that the proposed SSI damping controller successfully mitigates the SSI oscillations without deteriorating DFIG transient response.

The paper is organized as follows. The system description including DFIG wind turbines is presented in Section II. Section III briefly discusses the details of the system under study. The design of the proposed controller is given in Section IV. The effectiveness of the proposed controller and the transient behavior of the system are demonstrated through simulations in Section V, and Section VI concludes the paper.

II. WIND FARMS WITH DFIG WIND TURBINES

A simplified single line diagram of a typical wind farm is shown in Fig. 1. In such a wind farm, wind turbines (WTs) are connected through step-up transformers (not shown in Fig. 1) to the medium voltage (MV) collector bus by means of cables. The collector bus voltage is connected to the high voltage (HV) level via a wind farm step-up transformer. Depending on the selection of the function, either the reactive power, the voltage or the power factor at the POI, Fig. 1, is controlled by a central WFC located at the wind farm substation.

The following subsections briefly present DFIG-based WTs and reactive power control in wind farms. More details can be found in [14].

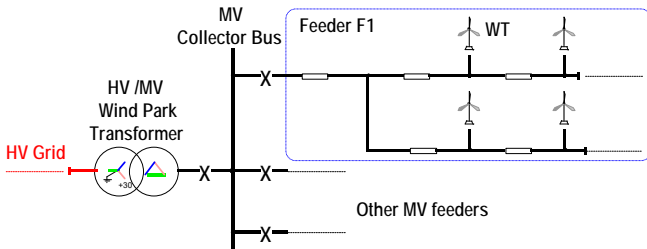


Fig. 1. A simplified single-line diagram of a typical wind farms.

A. DFIG Wind Turbines

In DFIG WTs, the stator of the induction generator (IG) is directly connected to the grid. However, the wound rotor is interfaced to the grid through a back-to-back converter system, as shown in Fig. 2. The back-to-back converter consists of two three-phase voltage-sourced converters (RSC and GSC), coupled through a common DC bus. A line inductor and a shunt harmonic AC filter are used by the GSC to improve power quality. A crowbar (not shown in Fig. 2) is used to protect the RSC against overcurrent, and the DC capacitor against overvoltage. During crowbar ignition, the RSC is blocked and the IG consumes reactive power. To avoid the crowbar ignition during faults, a DC resistive chopper is widely used to limit the DC voltage.

The DFIG WT is controlled using vector control techniques of the RSC and GSC. Vector control provides decoupled control of real and reactive powers. The currents are projected on a rotating reference frame based on either AC flux or voltage.

The control scheme is illustrated in Fig. 3, where i_{qr} and i_{dr} are the q- and d-axis currents of the RSC, i_{qg} and i_{dg} are the q- and d-axis currents of the GSC, V_{dc} is the DC bus voltage, P_{dfig} is the active power output of DFIG, and V_{dfig} is the positive-sequence of the DFIG terminal voltage. In Fig. 3 and hereafter, the apostrophe sign is used to indicate the reference values.

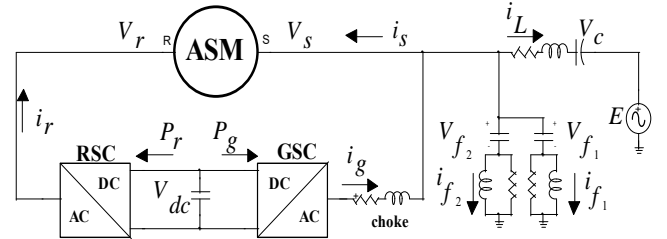


Fig. 2. Radially compensated wind farm model used in eigenvalue analysis.

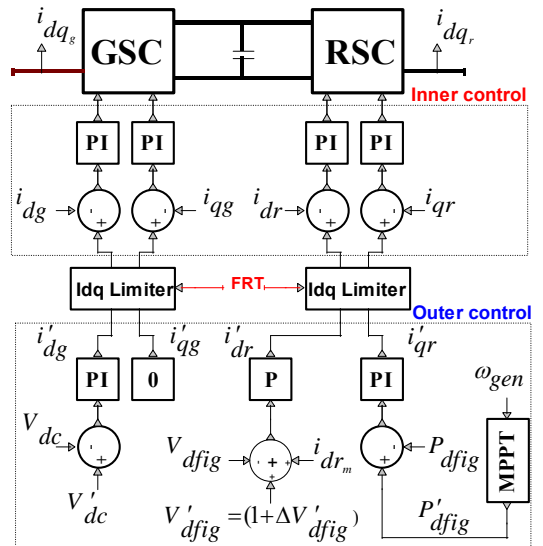


Fig. 3. Schematic diagram of DFIG wind turbine control.

In the control scheme of Fig. 3, the RSC operates in the stator flux reference (SFR) frame, and the GSC operates in the stator voltage reference (SVR) frame. The DFIG power P_{dfig} and its voltage V_{dfig} are controlled using i_{qr} and i_{dr} , respectively. On the other hand, i_{dg} is used to regulate the DC bus voltage V_{dc} and i_{qg} is used to support the grid with reactive power during faults. Both RSC and GSC include two control loops, namely, outer loop and inner loop controllers. The slow outer control generates the reference signals for the dq-frame currents (i'_{dr} , i'_{qr} , i'_{dg} and i'_{qg}), and the fast inner loop allows control of the converter AC voltage that will be used to generate the modulated switching pattern. The reference for DFIG active power output (P'_{dfig}) is determined by a maximum power point tracking (MPPT) algorithm. The reference for the DFIG positive-sequence voltage (V'_{dfig}) is calculated by WFC.

In Fig. 3, i_{dr_m} is the compensating term for the reactive current absorbed by the IG and approximated by

$$i_{dr_m} = V_{dfig} / X_m \quad (1)$$

where X_m is the IG magnetizing reactance.

During normal operation, GSC operates at unity power factor ($i'_{qg} = 0$) and the RSC controller gives the priority to the active current, i.e.

$$\begin{aligned} i'_{dr} &< I_{dr}^{\lim}, & I_{dr}^{\lim} &= 1 \text{ pu} \\ i'_{qr} &< I_{qr}^{\lim} = \sqrt{(I_r^{\lim})^2 - (i'_{dr})^2}, & I_r^{\lim} &= 1.1 \text{ pu} \end{aligned} \quad (2)$$

where I_{dr}^{\lim} , I_{qr}^{\lim} and I_r^{\lim} are the limits for d-axis, q-axis and total RSC currents, respectively.

B. Reactive Power Control in Wind Farms

The reactive power control in a wind farm is based on the secondary voltage control concept [14]. The outer control of the WTs includes a proportional voltage control (Fig. 3), which follows the voltage references determined and transmitted by the WFC shown in Fig. 4. The desired reactive power flow at the POI is achieved by the proportional-integral (PI) regulator of the WFC.

Although not shown in Fig. 4, the WFC may also contain voltage control (V-control) and power factor control (PF-control) functions. When the WFC is working under V-control function, the reactive power reference in Fig. 4 (Q'_{POI}) is calculated by an outer proportional voltage control, i.e.

$$Q'_{POI} = K_{V_{poi}} (V'_{POI} - V_{POI}) \quad (3)$$

where V_{POI} is the positive-sequence voltage at the POI and $K_{V_{poi}}$ is the gain of the WFC voltage regulator.

When the WFC is operating under PF-control function, Q'_{POI} is calculated using the active power at the POI (P_{POI}) and the desired power factor at the POI (PF'_{POI}).

When a severe voltage sag occurs at the POI (e.g., due to a fault), the PI regulator output ($\Delta V'_{dfig}$) is kept constant by blocking the input ($Q'_{POI} - Q_{POI}$) to avoid overvoltage following the fault removal.

This paper considers only WFC operating under Q-control function due to space limitations. It should be noted that, operating under V-control or PF-control does not have noticeable impact on SSI due to the slow response of the WFC reactive power regulator.

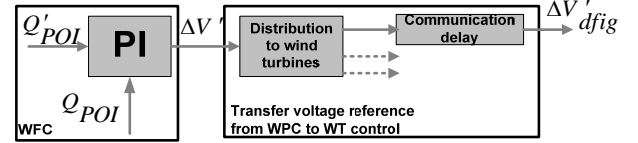


Fig. 4. Reactive power control at the POI.

C. Fault-Ride-Through (FRT) Function

In order to fulfill the grid code requirement regarding voltage support shown in Fig. 5, the WTs are equipped with an FRT function. In this figure, $I_{reactive}$ is the reactive current of the DFIG. The FRT function is activated when the voltage deviation ($V_{dfig} - 1$) pu exceeds the pre-defined value, V_{FRT-ON} , and it is deactivated when the voltage deviation goes below the pre-defined value, $V_{FRT-OFF}$, after a pre-specified release time, t_{FRT} .

During FRT operation the RSC controller gives the priority to the reactive current by reversing the d- and q-axis current limits given in (2). Moreover, GSC starts injecting reactive currents during faults when the RSC reactive current contribution is not sufficient to satisfy the grid code requirement due to the reactive current absorbed by the IG. More details can be found in [14].

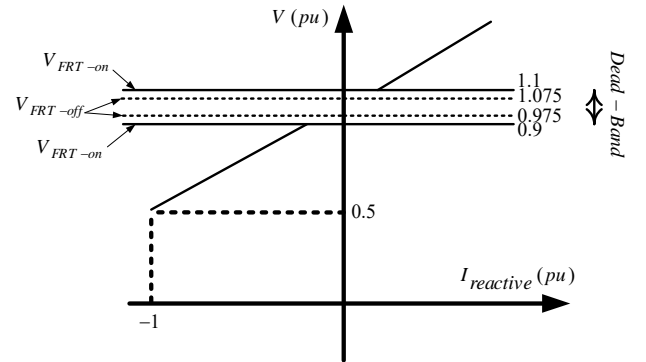


Fig. 5. Reactive power control at the POI.

III. SYSTEM UNDER STUDY

To evaluate the effectiveness of the proposed SSI mitigation method, the system shown in Fig. 6 is adopted as a test benchmark.

The considered DFIG-based wind farm, shown in Fig. 6, comprises 266 wind turbines; each with the rating of 1.5 MW and 0.575 kV. This power system is inspired from an actual one that includes two 500 kV transmission lines designated as lines

A and B. Line A (500 km) is series compensated by two identical capacitor banks located at its ends that provide a 50% compensation degree. Line A also contains 230 MVAR shunt reactors at both ends. Lines A and B (100 km) are connected to two large systems and represented with distributed constant parameter models in EMT simulations. B1 and B2 are the circuit breakers of Line B. **The operating times for the close and remote breakers are 60 ms and 80 ms, respectively.** Disconnection of Line B leaves the wind farm radially connected to the series capacitor compensated transmission line. The electrical system seen from DFIG terminals has a reactance crossover at 30 Hz as shown in Fig. 7.

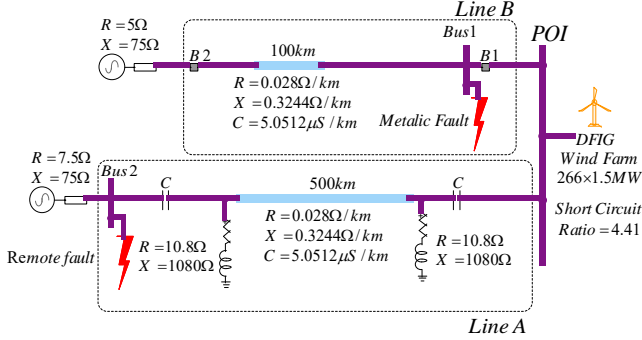


Fig. 6. The case study system

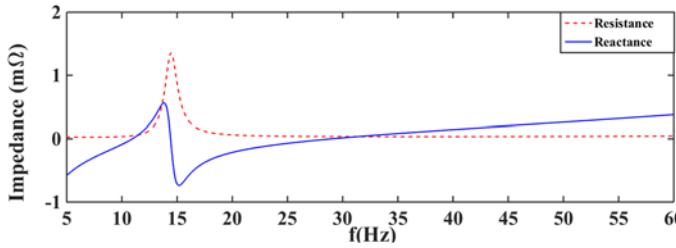


Fig. 7. Impedance seen from DFIG terminals.

IV. CONTROL DESIGN

This section briefly presents a linearized model for the system, and presents a detailed procedure for the SSI damping control design.

A. Linearization

The radially compensated wind farm model used in eigenvalue analysis and SSI damping controller design is shown in Fig. 2. The external electrical network (i.e., the series capacitor compensated transmission line, the wind farm transformer, the equivalent collector grid and the aggregated DFIG transformers) is represented with a single RLC branch. All shunt branches in the electrical system are disregarded except the DFIG aggregated harmonic filters.

The linearized state-space representation of the IG, external electrical network (RLC branch in Fig. 2), choke filter, DC bus and torsional dynamics can be found in [14],[18]. Due to space limitation, the linearization procedure is not given here.

The DFIG converters behave like a controlled voltage source and directly regulate their output currents. The inner current control loop of the RSC is expressed as

$$\begin{aligned} v_{dr} &= (K_{Pr} + K_{Ir}/s)(i'_{dr} - i_{dr}) + FF_{dr} \\ v_{qr} &= (K_{Pr} + K_{Ir}/s)(i'_{qr} - i_{qr}) + FF_{qr} \end{aligned} \quad (4)$$

where v_{dr} and v_{qr} are the RSC terminal voltages, K_{Pr} and K_{Ir} are the PI control parameters. FF_{dr} and FF_{qr} are the feedforward signals whose detailed expressions can be found in [14],[18]. The outer loops provide the references for the inner loops for both RSC and GSC. The outer loop equations of the RSC are:

$$\begin{aligned} i'_{dr} &= (K_v)(1 + \Delta V'_{dfig} - V_{dfig}) + i_{dr-m} \\ i'_{qr} &= (K_{pp} + K_{Ip}/s)(P'_{dfig} - P_{dfig}) \end{aligned} \quad (5)$$

where K_v is the gain of the voltage regulator, and K_{pp} and K_{Ip} are the parameters of the PI regulator in q-axis direction. The MPPT algorithm provides the reference for the active power control.

Similarly, the inner current control loop of the GSC is expressed as:

$$\begin{aligned} v_{dg} &= (K_{Pg} + K_{Ig}/s)(i'_{dg} - i_{dg}) + FF_{dg} \\ v_{qg} &= (K_{Pg} + K_{Ig}/s)(i'_{qg} - i_{qg}) + FF_{qg} \end{aligned} \quad (6)$$

where v_{dg} and v_{qg} are the GSC terminal voltages, K_{Pg} and K_{Ig} are the PI parameters, and FF_{dg} and FF_{qg} are the feedforward signals as detailed in [14].

The GSC outer loop regulates the DC link voltage and has the following structure:

$$i'_{dg} = (K_{Pdc} + K_{Idc}/s)(V'_{dc} - V_{dc}) \quad (7)$$

where the K_{Pdc} and K_{Idc} are the PI controller parameters. The reference current i'_{qg} is set to zero as GSC operates at unity power factor during normal operation.

B. LQR Design

The LQR method [19] provides the optimal state variable feedback (SVFB) control for a linear system represented by

$$\begin{aligned} \dot{\mathbf{x}} &= \mathbf{A}\mathbf{x} + \mathbf{B}\mathbf{u} \\ \mathbf{y} &= \mathbf{C}\mathbf{x} + \mathbf{D}\mathbf{u} \end{aligned} \quad (8)$$

Where \mathbf{x} , \mathbf{u} and \mathbf{y} are the state vector, control input and system outputs, respectively. The matrices \mathbf{A} , \mathbf{B} , \mathbf{C} and \mathbf{D} are obtained from the linearization process and describe the small signal behavior of the system. The optimal feedback (control) signal ($\mathbf{u} = -\mathbf{K}\mathbf{x}$) is determined through a cost function by selecting a positive-definite input matrix \mathbf{R} and a positive-semidefinite state matrix \mathbf{Q} [19]. The matrices \mathbf{R} and \mathbf{Q} determine a trade-off between the energy of the control signals and energy of the controlled output. In our design, we set $\mathbf{Q} = \mathbf{C}^T \mathbf{C}$ and \mathbf{R} is obtained using the time-domain simulations considering the WT behavior and the energy of the SVFB signals when the system is subject to large disturbances. It should be noted that the large values of \mathbf{R} result in small static gains \mathbf{K} for the SVFB.

C. Observer Design

In a practical situation, all state variables may not be accessible or measurable. Hence, the SVFB implementation requires a state observer:

$$\dot{\hat{\mathbf{x}}} = \mathbf{A}\hat{\mathbf{x}} + \mathbf{B}\mathbf{u} + \mathbf{L}(\mathbf{y} - \mathbf{C}\hat{\mathbf{x}}) \quad (9)$$

where \mathbf{L} is the observer gain and $\hat{\mathbf{x}}$ denotes the estimated state vector. The matrix \mathbf{L} determines the dynamic behavior of observer, i.e., the estimation speed (or the dynamic of error $\mathbf{e} = \mathbf{x} - \hat{\mathbf{x}}$) depends on the loci of the eigenvalues of $\mathbf{A} - \mathbf{L}\mathbf{C}$.

In this paper, the LQR and LMI techniques are used to design an optimal gain for the observer. The similar approach discussed in IV-B [19] is used to design the LQR based observer.

The LMI based technique enables the designer to assign the eigenvalues of the matrix $\mathbf{A} - \mathbf{L}\mathbf{C}$ (error dynamic) in a prescribed LMI region, Fig. 8 [20]. In order to achieve fast transient response for the overall closed-loop system, the observer should be designed much faster than the closed-loop system without observer. However, very fast observer results in a control system sensitive to measurement noise.

Let D be an arbitrary LMI region in the s -plane as:

$$D = \{s \mid s \in \mathbb{C}, \mathbf{N} + s\mathbf{M} + \bar{s}\mathbf{M}^T < \mathbf{0}\} \quad (10)$$

where s is the Laplace variable, \mathbb{C} is the set of complex numbers, and \mathbf{N} and \mathbf{M} are some real matrices which specify the LMI region D .

The closed-loop system is D -stable (i.e., the closed-loop poles lie in the region D) if and only if there exists a symmetric positive-definite matrix \mathbf{P}_{LMI} such that the following generalized Lyapunov inequality holds [20],[21]:

$$\mathbf{L} \otimes \mathbf{P}_{\text{LMI}} + \mathbf{M} \otimes (\mathbf{A}\mathbf{P}_{\text{LMI}}) + \mathbf{M}^T \otimes (\mathbf{A}\mathbf{P}_{\text{LMI}})^T < \mathbf{0} \quad (11)$$

In (11), \otimes denotes the Kronecker product for the matrices. This paper considers the LMI region given in Fig. 8. The corresponding observer gain matrix \mathbf{L} is designed based on the method discussed in [20]:

$$\mathbf{L} = (\mathbf{W}\mathbf{P}_{\text{LMI}}^{-1})^T \quad (12)$$

where

$$\mathbf{A}^T \mathbf{P}_{\text{LMI}} + \mathbf{A} \mathbf{P}_{\text{LMI}} - \mathbf{C}^T \mathbf{W} - \mathbf{W}^T \mathbf{C} + 2\alpha \mathbf{P}_{\text{LMI}} < \mathbf{0} \quad (13)$$

$\mathbf{P}_{\text{LMI}} > \mathbf{0}$ and α is the distance between the imaginary axis and the desired LMI region D , as shown in Fig. 8.

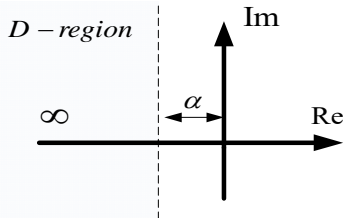


Fig. 8. Observer pole placement region.

D. SSI Damping Control Design

The SSI damping controller is designed considering the radially compensated DFIG-based wind farm shown in Fig. 2

and its linearized equations given in (10). The state vector consists of:

$$\mathbf{x} = [\mathbf{x}_{dc} \ \mathbf{x}_{IG} \ \mathbf{x}_{mech} \ \mathbf{x}_{choke} \ \mathbf{x}_{Line} \ \mathbf{x}_{HF} \ \mathbf{x}_{CNTL} \ \mathbf{x}_{VF} \ \mathbf{x}_{IF} \ \mathbf{x}_{dcF}]^T \quad (14)$$

where $\mathbf{x}_{dc} \in \mathbb{R}$ is the DC link voltage, the state vector $\mathbf{x}_{IG} \in \mathbb{R}^{1 \times 4}$ contains the stator and rotor currents, $\mathbf{x}_{mech} \in \mathbb{R}^{1 \times 3}$ represents the state vector of two-mass WT shaft model, $\mathbf{x}_{choke} \in \mathbb{R}^{1 \times 2}$ is the vector of currents of the choke, $\mathbf{x}_{Line} \in \mathbb{R}^{1 \times 4}$ represents the line current and series capacitor voltage, $\mathbf{x}_{HF} \in \mathbb{R}^{1 \times 8}$ denotes the capacitor voltages and inductance currents of the harmonic filter and $\mathbf{x}_{CNTL} \in \mathbb{R}^{1 \times 6}$ denotes the state vector of WT controllers. $\mathbf{x}_{dcF} \in \mathbb{R}^{1 \times 2}$ represents the states of the second order low pass filter used to filter the DC link voltage. The cut-off frequency of this filter is 282 Hz. $\mathbf{x}_{VF} \in \mathbb{R}^{1 \times 2}$ and $\mathbf{x}_{IF} \in \mathbb{R}^{1 \times 2}$ are the filtered DFIG dq-frame voltages and currents, respectively. Those filter are first order low pass filters with cut-off frequency 21.21 Hz. The filtered DFIG dq-frame voltages and currents are used to calculate the terminal voltage and the output power used by the outer control.

$$V_{dfig} = \sqrt{V_{dfig-df}^2 + V_{dfig-qf}^2} \quad (15)$$

$$P_{dfig} = (V_{dfig-df} I_{dfig-df} + V_{dfig-qf} I_{dfig-qf}) \quad (16)$$

where $V_{dfig-df}$, $V_{dfig-qf}$ are the filtered DFIG dq-frame voltages and $I_{dfig-df}$, $I_{dfig-qf}$ are the DFIG dq-frame currents.

Similar to WFC, the supplementary SSI damping controller is located at the wind farm substation. The proposed observer uses only the DFIG converter currents (i.e. $\mathbf{y} = [i_{qr} \ i_{dr} \ i_{qs} \ i_{ds}]^T$) and eliminates the communication requirement between the SSI damping controller and the external power system. The SSI damping controller output signals are added to the current references produced by the outer control of RSC and GSC, and limited dynamically to ensure the desired DFIG active and reactive current outputs during normal and FRT operations, respectively.

Disconnection of Line B in the considered system (as shown in Fig. 6) leaves the wind farm radially connected to the series capacitor compensated transmission line. For various wind speeds and Line B outage scenario, the impact of the wind farm reactive power and the WT outages on SSI mode is illustrated in Fig. 9 and Fig. 10, respectively. The impact of the wind farm reactive power generation on SSI mode damping is not significant. However, SSI mode damping reduces with the wind speed and most severe SSI problem is expected at slowest permissible wind speed when there is 150 WTs in service.

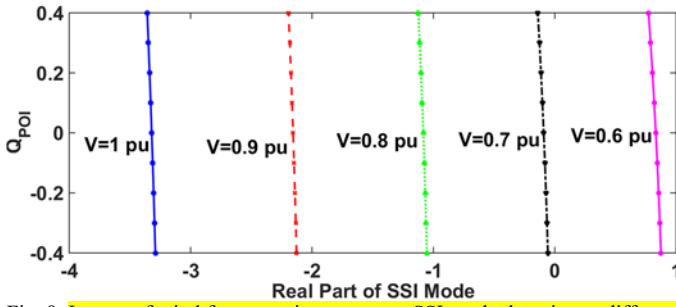


Fig. 9. Impact of wind farm reactive power on SSI mode damping at different wind speeds.

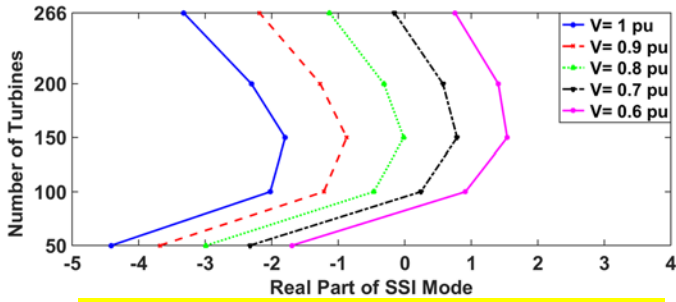


Fig. 10. Impact wind turbine outages on SSI mode damping at different wind speeds.

Although not presented here, representative EMT simulations are performed to validate the eigenvalue analysis results. The EMT simulation results correlate with eigenvalue analysis results. However, the SSI mode dampings in EMT simulations are slightly lower compared to the SSI mode dampings obtained in eigenvalue analysis. It should be noted that, the linearized system model presented in Section IV.A disregards the low pass measuring filters and PLL dynamics.

The SSI damping controller is designed for slowest permissible wind speed and no WT outage scenario.

V. EMT SIMULATIONS

The performance of the proposed SSI damping controller is tested via EMT simulations using EMTP-RV [22]. In all scenarios, the wind speed is 0.6 pu (i.e. the slowest permissible wind speed) and the wind farm is operating with unity power factor (i.e. $Q_{poi} = 0$). In scenarios S1 and S2, all WTs are in service. In scenario S3, 150 WTs are in service.

S1. A three-phase metallic fault is applied at BUS1 end of Line B at $t = 1$ s (electrically close fault). The fault is cleared with the operation of circuit breakers B1 and B2 (as shown in Fig. 6).

S2. An electrically distant fault condition is imitated by applying three-phase fault at BUS2 with an impedance of 0.3162Ω ($X/R = 3$) at $t = 1$ s and removed at $t = 1.3$ s. Long fault clearing time (0.3 s) imitates delayed operation of the protection system due to either breaker failure or disoperation of protection system.

S3. The distant fault in scenario S2 is applied at $t = 4$ s following the close fault in S1.

It should be noted that, scenario S2 is repeated for a wide range of fault impedances which results in 0.5 pu to 0.8 pu voltage sag at DFIG terminals. Only one of the simulated

scenarios is presented here due to space limitation. However, the SSI damping controller performance is similar in all other fault impedance cases.

A. Scenario S1

The presented waveforms in Fig. 11 confirm the effectiveness of the proposed SSI damping controller. The system remains stable after disconnection of Line B following the fault. The damping controller exhibits similar performance with both LMI and LQR based observers.

When the SSI damping controller output is blocked during FRT operation as proposed in [7], its performance reduces slightly compared to the proposed dynamic limitation approach as shown in Fig. 12. The reactive power output and terminal voltage of DFIG during fault are similar in both SSI damping controller output restriction schemes. In other words, the DFIG supplies the desired reactive currents during fault.

B. Scenario S2

In this scenario, the SSI mode has negative damping during fault even with the proposed SSI damping controller (as shown in Fig. 13). However, that transient SSI problem is less severe with the proposed damping controller. Moreover, the system becomes stable after fault removal with the proposed mitigation. The performance of the proposed damping controller is slightly better with LMI based observer compared to LQR based observer.

When the SSI damping controller output is blocked during FRT operation as proposed in [7], the damping controller remains blocked after the fault removal as the FRT operation continues due to large magnitude oscillations at measured positive sequence terminal voltage V_{dfig} (as shown in Fig. 14). As a result, the SSI mode remains undamped.

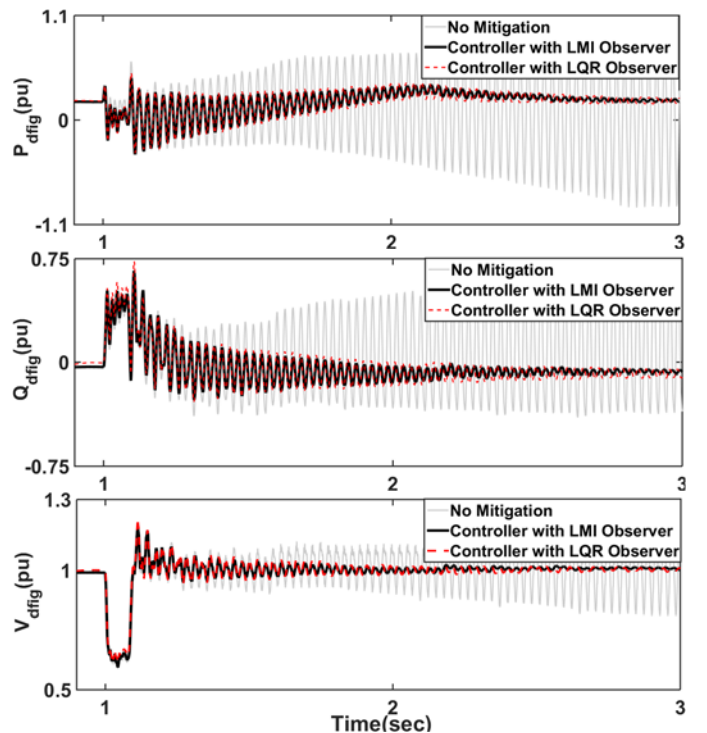


Fig. 11. DFIG active power, reactive power and terminal voltage in S1

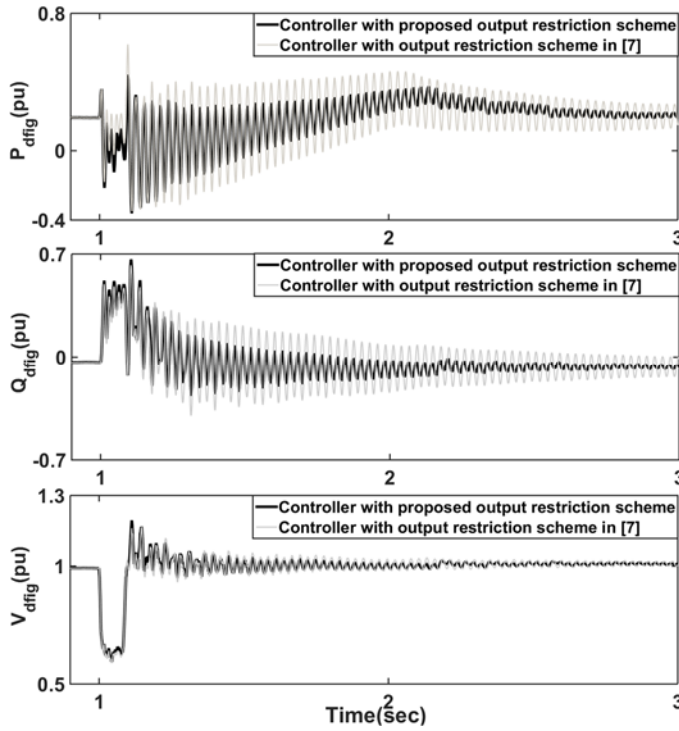


Fig. 12. DFIG active power, reactive power and terminal voltage in S1 for different SSI damping controller output restriction schemes (with LMI observer).

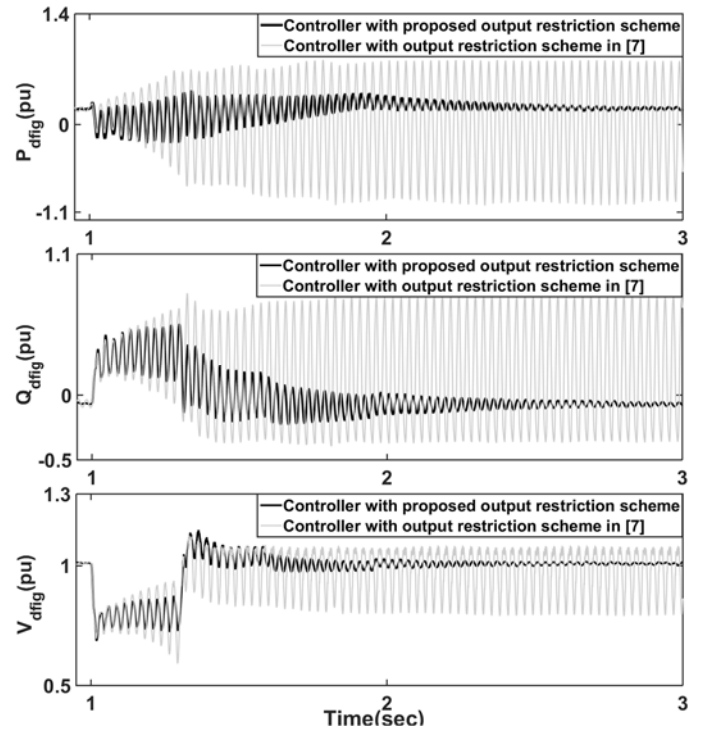


Fig. 14. DFIG active power, reactive power and terminal voltage in S1 for different SSI damping controller output restriction schemes (with LMI observer).

C. Scenario S3

The fault scenarios in S1 and S2 are simulated for the WT outage scenario in which the SSI problem is the most severe. Only the SSI damping controller with LMI observer is considered in this scenario, as it exhibits better performance in both S1 and S2. The waveforms presented in Fig. 15 and 16 confirm the effectiveness of the proposed damping controller.

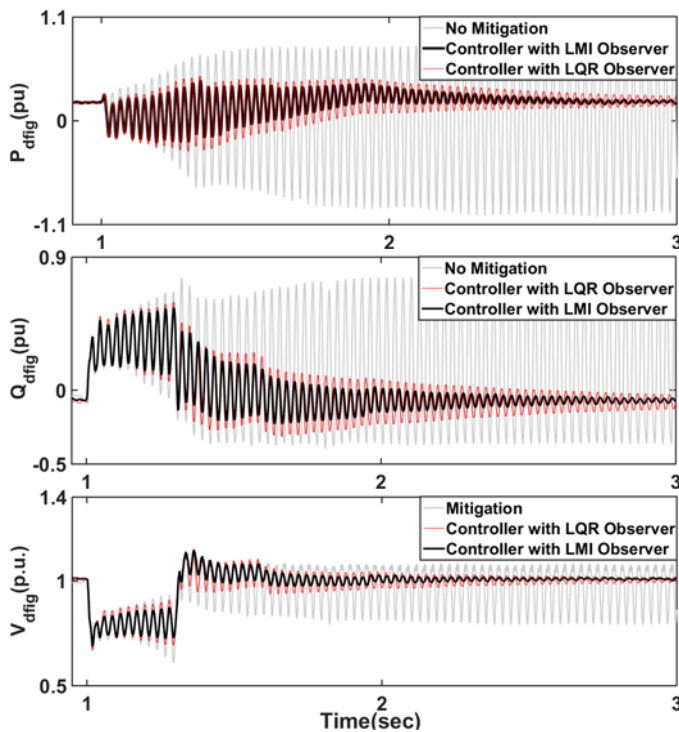


Fig. 13. DFIG active power, reactive power and terminal voltage in S2.

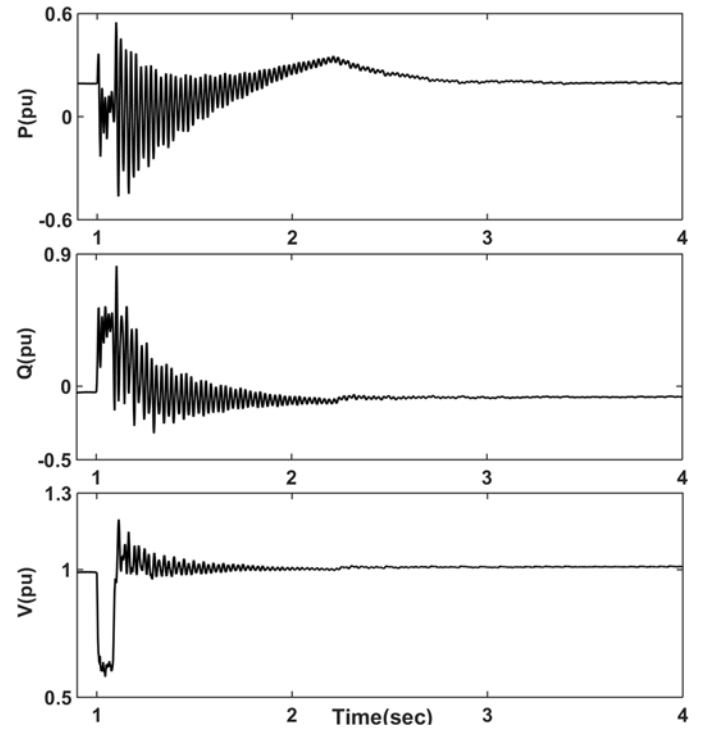


Fig. 15. DFIG active power, reactive power and terminal voltage in S3 (response to electrically close fault).

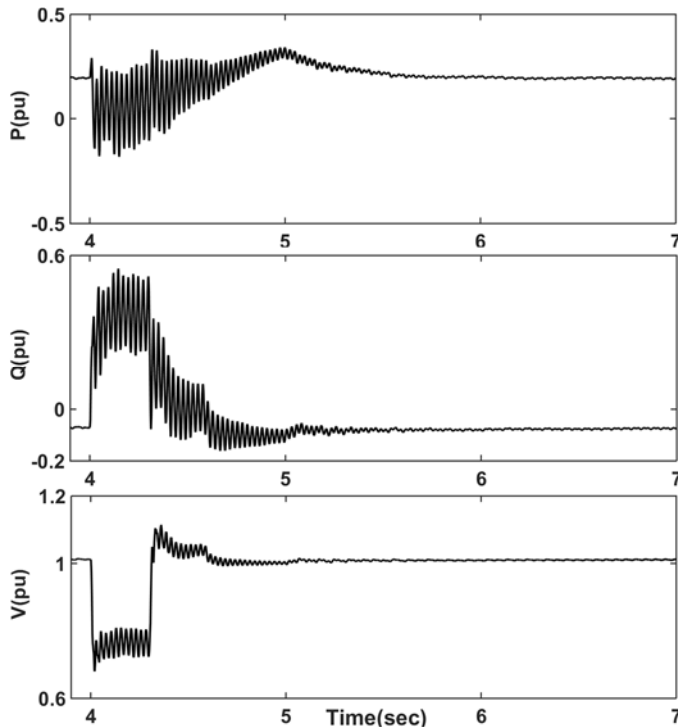


Fig. 16. DFIG active power, reactive power and terminal voltage in S3 (response to electrically distant fault).

VI. CONCLUSION

This paper proposed a central MIMO LQR based SSI damping controller for series compensated DFIG based wind farms. The proposed SSI damping controller uses a full state observer in SVFB implementation and requires only the RSC and GSC currents of the DFIGs as its inputs. The LMI technique is used to design the observer gain. The output signals of the proposed controller are supplemented to the inner current control loops of the DFIG converters, and limited dynamically considering the DFIG converter limits and the desired DFIG transient response to the faults. The SSI damping controller is designed for a practical series compensated wind farm using the linearized system model, and tested with EMT simulations using detailed DFIG model that include the nonlinearities and the essential transient functions to fulfill the grid code requirement regarding FRT.

The simulation scenarios include the extreme wind farm operating conditions where the SSI problem is the most severe and also the extreme fault conditions where the faulted system has an undamped SSI mode. The EMT simulations demonstrated that the proposed controller provides desired SSI damping without significant deterioration in DFIG transient response.

REFERENCES

- [1] L. Fan, C. Zhu, Z. Miao and M. Hu, "Modal Analysis of a DFIG-Based Wind Farm Interfaced With a Series Compensated Network," in *IEEE Transactions on Energy Conversion*, vol. 26, no. 4, pp. 1010-1020, Dec. 2011.
- [2] G. D. Irwin, A. K. Jindal and A. L. Isaacs, "Sub-synchronous control interactions between Type 3 wind turbines and series compensated AC transmission systems," *2011 IEEE Power and Energy Society General Meeting*, San Diego, CA, 2011, pp. 1-6.

- [3] M. Sahni *et al.*, "Sub-synchronous interaction in Wind Power Plants- part II: An ertcot case study," *2012 IEEE Power and Energy Society General Meeting*, San Diego, CA, 2012, pp. 1-9.
- [4] J. Adams, C. Carter and S. H. Huang, "ERCOT experience with Sub-synchronous Control Interaction and proposed remediation," *Transmission and Distribution Conference and Exposition (T&D), 2012 IEEE PES*, Orlando, FL, 2012, pp. 1-5.
- [5] A. E. Leon and J. A. Solsona, "Sub-Synchronous Interaction Damping Control for DFIG Wind Turbines," in *IEEE Transactions on Power Systems*, vol. 30, no. 1, pp. 419-428, Jan. 2015.
- [6] R. K. Varma, S. Auddy and Y. Semsedini, "Mitigation of Subsynchronous Resonance in a Series-Compensated Wind Farm Using FACTS Controllers," in *IEEE Transactions on Power Delivery*, vol. 23, no. 3, pp. 1645-1654, July 2008.
- [7] U. Karaagac, S. O. Faried, J. Mahseredjian and A. A. Edris, "Coordinated Control of Wind Energy Conversion Systems for Mitigating Subsynchronous Interaction in DFIG-Based Wind Farms," in *IEEE Transactions on Smart Grid*, vol. 5, no. 5, pp. 2440-2449, Sept. 2014.
- [8] H. A. Mohammadpour and E. Santi, "SSR Damping Controller Design and Optimal Placement in Rotor-Side and Grid-Side Converters of Series-Compensated DFIG-Based Wind Farm," in *IEEE Transactions on Sustainable Energy*, vol. 6, no. 2, pp. 388-399, April 2015.
- [9] C. Zhu, L. Fan and M. Hu, "Control and analysis of DFIG-based wind turbines in a series compensated network for SSR damping," *IEEE PES General Meeting*, Minneapolis, MN, 2010, pp. 1-6.
- [10] L. Fan and Z. Miao, "Mitigating SSR Using DFIG-Based Wind Generation," in *IEEE Transactions on Sustainable Energy*, vol. 3, no. 3, pp. 349-358, July 2012.
- [11] P. H. Huang, M. S. El Moursi, W. Xiao and J. L. Kirtley, "Subsynchronous Resonance Mitigation for Series-Compensated DFIG-Based Wind Farm by Using Two-Degree-of-Freedom Control Strategy," in *IEEE Transactions on Power Systems*, vol. 30, no. 3, pp. 1442-1454, May 2015.
- [12] A. E. Leon and J. A. Solsona, "Sub-Synchronous Interaction Damping Control for DFIG Wind Turbines," in *IEEE Transactions on Power Systems*, vol. 30, no. 1, pp. 419-428, Jan. 2015.
- [13] L. Fan, R. Kavasseri, Z. Miao and C. Zhu, "Modeling of DFIG-Based Wind Farms for SSR Studies," in *IEEE Transactions on power delivery*, vol. 25, no. 4, pp. 2073-2082, October 2010.
- [14] U. Karaagac, H. Saad, J. Peralta, J. Mahseredjian, "Doubly-fed induction generator based wind park models in EMT-P-RV," April 2015.
- [15] "Grid code - high and extra high voltage," E.ON Netz GmbH, Bayreuth, Germany, April 2006.
- [16] S. Nallusamy, D. Velayutham and U. Govindarajan, "Design and implementation of a linear quadratic regulator controlled active power conditioner for effective source utilisation and voltage regulation in low-power wind energy conversion systems," in *IET Power Electronics*, vol. 8, no. 11, pp. 2145-2155, 11 2015.
- [17] H. S. Ko and J. Jatskevich, "Power Quality Control of Wind-Hybrid Power Generation System Using Fuzzy-LQR Controller," in *IEEE Transactions on Energy Conversion*, vol. 22, no. 2, pp. 516-527, June 2007.
- [18] L. Fan and Z. Miao, Modeling and Analysis of Doubly Fed Induction generator Wind Energy Systems, Academic Press, April 2015.
- [19] S. Skogestad and I. Postlethwaite, "Multivariable Feedback Control, Analysis and Design," Wiley, Nov 4, 2005.
- [20] G.R.Duan, H. H. Yu, "LMIs in Control Systems: Analysis, Design and Applications," CRC Press, Jun 2013.
- [21] M. Chilali, P. Gahinet, P. Apkarian, "Robust pole placement in LMI regions," in *Automatic Control*, *IEEE Transactions on*, vol.44, no.12, pp.2257-2270, Dec 1999.
- [22] J. Mahseredjian, S. Denneri, L. Dubé, B. Khodabakhchian and L. Gérin-Lajoie, "On a new approach for the simulation of transients in power systems". *Electric Power Systems Research*, Volume 77, Issue 11, September 2007, pp. 1514-1520.

APPENDIX A

The wind farm parameters are summarized in Table I.

TABLE I
WIND FARM PARAMETERS

Parameter	Value	Parameter	Value
$S_{DFIG_transformer}$	1.75 MVA	$T_{RSC-risetime}$	20 ms
$R_{DFIG_transformer}$	0.002	$T_{GSC-risetime}$	10 ms
$X_{DFIG_transformer}$	0.06 pu	K_V	2
$S_{wind\ farm_transformer}$	444MVA	K_P	1
$R_{wind\ farm_transformer}$	0.005	$DFIG_{poles}$	6
$X_{wind\ farm_transformer}$	0.15 pu	R_s	0.033
$R_{Collector}$	0.02 ohm	R_r	0.026
$X_{Collector}$	0.06 mH	L_{md}	2.9 pu
$C_{Collector}$	47uF	L_{mq}	2.9 pu
H_{gen}	0.9 pu	L_{ls}	0.18
D_{gen}	0 pu	L_{lr}	0.16
K_{shaft}	1.2 pu	V_{dc}	1150 V
D_{shaft}	1.5 pu	R_{choke}	0.015pu
$H_{turbine}$	4 s	X_{choke}	1.5 pu